Jiao and Chawla *Integrating Materials and Manufacturing Innovation* 2014, **3**:3
http://www.immijournal.com/content/3/1/3

Integrating Materials and Manufacturing Innovation
a SpringerOpen Journal

RESEARCH Open Access

Three dimensional modeling of complex heterogeneous materials via statistical microstructural descriptors

Yang Jiao* and Nikhilesh Chawla

* Correspondence:
yang.jiao.2@asu.edu
Materials Science and Engineering, Arizona State University, Tempe, AZ 85287-6206, USA

Abstract

Heterogeneous materials have been widely used in many engineering applications. Achieving optimal material performance requires a quantitative knowledge of the complex material microstructure and structural evolution under external stimuli. Here, we present a framework to model material microstructure via statistical morphological descriptors, i.e., certain lower-order correlation functions associated with the material's phases. This allows one to reduce the large data sets for a complete specification of all of the local states in a microstructure to a handful of simple scalar functions that statistically capture the salient structural features of the material. Stochastic reconstruction techniques can then be employed to investigate the information content of the correlation functions, suggest superior and sensitive structural descriptors as well as generate realistic virtual 3D microstructures from the given limited structural information. The framework is employed to successfully model a variety of materials systems including an anisotropic aluminium alloy, a polycrystalline tin solder, the structural evolution in a binary lead-tin alloy when aged, and a model structure of hard-sphere packing. Our framework also has ramifications in the development of integrated computational material design schemes and 4D materials modeling techniques.

Keywords: Heterogeneous materials; 3D microstructure modeling; Statistical structural descriptors; Stochastic reconstruction

Background

Heterogeneous materials including metallic alloys, ceramics, composites and granular media have many important engineering applications. Such materials possess complex microstructures spanning a wide spectrum of length scales, which determine their macroscopic properties and performance [1-4]. The growing demands in global sustainability, national security, and renewable energy have raised great challenges in the development of multifunctional materials that can achieve optimal performance under extreme conditions [5,6]. The success of such a mission strongly relies on our ability to characterize and modify material properties and behaviors under a myriad of external stimuli. Thus, an intrinsic understanding and knowledge of complex microstructures and how they evolve under various conditions is extremely important.

Advances in experimental methods, analytical techniques, and computational approaches, have now enabled the development of three dimensional (3D) analyses [7].

Figure 1 illustrates the characterization of the microstructure of a Sn-3.5Ag eutectic alloy, a candidate lead-free solder for electronic packaging, by tomographic microscopy across a wide range of length scales. The study of 3D microstructures under an external stimulus (e.g., stress, temperature, environment) as a function of time (4D) is particularly exciting. Examples include an understanding of time-dependent deformation structures, phase transformations, compositional evolution, magnetic domains, etc. Furthermore, advances in 3D and 4D computational tools and methods have enabled the analysis of large experimental data sets, as well as simulation and prediction of material behavior [8-10], which we will briefly discuss in Methods.

X-ray tomography is an extremely attractive, non-destructive technique for characterizing microstructures in 3D and 4D. The use of high brilliance and partially coherent synchrotron light allows one to image multi-component materials from the sub-micrometer to nanometer range. X-ray tomography can be conducted in imaging modes based on absorption or phase contrast. The technique can also be used using lab-scale systems. To construct an accurate 3D microstructure model, 2D projections are obtained at small angular increments. Given a sufficiently large number of such 2D projections, tomographic reconstruction techniques such as the filtered-back-projection algorithm [11] can be employed to generate a grayscale image of the material microstructure. Further segmentation and thresholding analysis are used to resolve details of individual material phases and produce accurate digital representations of the 3D microstructure. These 3D or 4D data sets can be used to quantify the microstructure, and/or can be used as an input for microstructure-based modeling. Thus, tomography is an excellent technique that eliminates destructive cross-sectioning, and allows for superior resolution and image quality with minimal sample preparation [12-19].

Experimentally obtained microstructural data are usually represented as a large array whose entries indicate the local states of the microstructure (e.g., the phase that a specific voxel belongs to). Although morphological details of a specific material can be contained in its microstructrual array, such information would not all be useful for macroscopic effective property analysis, which requires averaging over a sufficiently large number of material samples to yield meaningful and robust statistics. In the case where the entire course of microstructural evolution is of interest (e.g., during

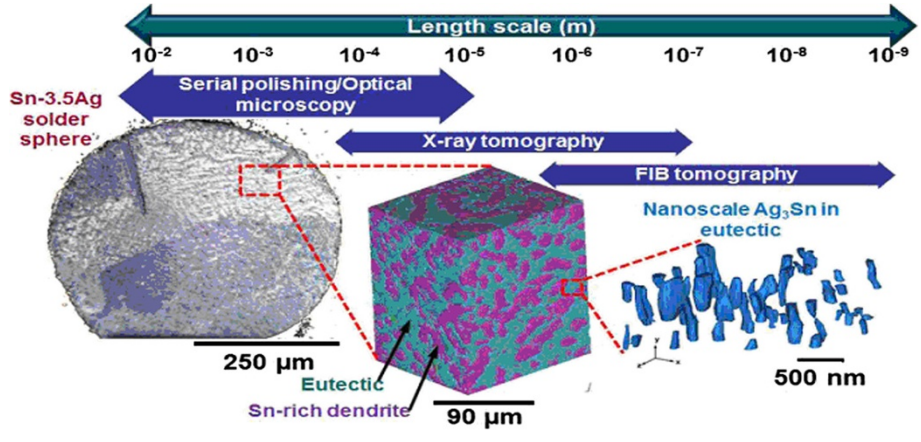

Figure 1 Characterization of the microstructure of Sn-3.5Ag eutectic alloy on multiple length scales via a variety of imaging techniques.

the solidification or coarsening processes), the resulting 4D structural data sets (three spatial dimensions plus one temporal dimension) are usually extremely large. In certain 4D cases, such as the progression of a fatigue crack over time, most of the material containing the crack remains unaltered and the major structural changes only occur in the vicinity of the crack tip [19]. Therefore, representing this process using a large number of reconstructed 3D microstructures at successive time points during the progression of the crack is less efficient and results in a huge amount of redundant structural information. Therefore, it is highly desirable to devise a robust framework that enables one to represent, characterize and model the complex microstructure of a heterogeneous material in 3D and 4D in a much more efficient manner.

Furthermore, for certain systems such as a polycrystalline material, it is still extremely difficult to directly obtain the 3D microstructure containing the information on grain misorientations using current imaging techniques. A common practice is to use serial sectioning to reconstruct the 3D material from 2D electron-back-scattered-diffraction (EBSD) images of the material's surfaces [20,21]. This technique, which involves extensive surface polishing, image smoothing and image alignment, is extremely time consuming and tedious. Thus, developing efficient statistical morphological descriptors that capture the key structural features of the materials from a handful of 2D images and that enable one to reconstruct accurate 3D virtual microstructure models from such limited information will significantly improve the efficiency in characterizing polycrystalline materials.

In this article, we present a framework to model the microstructure of complex heterogeneous materials via statistical morphological descriptors, i.e., certain lower-order correlation functions associated with the material's phases [3]. Such correlation functions are mainly derived from homogenization theories that quantitatively connect the macroscopic properties of a heterogeneous material to its complex microstructure [2-4]. Representing a microstructure with the combination of a selected set of correlation functions allows one to reduce the large data sets for a complete specification of all of the local states in a microstructure to a handful of simple scalar functions that statistically capture the salient structural features of the material [22-24]. Stochastic reconstruction techniques such as the simulated annealing procedure developed by Yeong and Torquato [25,26] can then be employed to investigate the information content of the correlation functions, suggest superior and sensitive structural descriptors as well as generate realistic virtual 3D microstructures from the given limited structural information. Material modeling based on correlation functions has enabled the development of data-driven material design schemes [27,28] and 4D materials modeling techniques [29].

The rest of the paper is organized as follows: In Statistical microstructural descriptors, we provide definitions of the statistical morphological descriptors (i.e., correlation functions) employed to model complex heterogeneous materials. In Methods, we present the Yeong-Torquato reconstruction procedure to generate virtual 3D microstructure models from a prescribed set of correlation functions. In Results, we apply our general framework and the reconstruction technique to model a variety of material systems, including an anisotropic aluminum alloy, a polycrystalline tin solder, as well as the 4D coarsening process of a lead-tin binary alloy. Concluding remarks are provided in Discussion and conclusion.

Statistical microstructural descriptors

In general, the microstructure of a heterogeneous material can be uniquely determined by specifying the indicator functions associated with all of the individual phases of the material [3], i.e.

$$I^{(i)}(\mathbf{x}) = \begin{cases} 1 & \mathbf{x} \text{ in phase } i \\ 0 & \text{otherwise} \end{cases} \tag{1}$$

where i =1, ..., q and q is the total number of phases. In practice, a digitized version of the indicator function, i.e., a 3D array whose entries specifying the phases that the voxels belong to, is used to fully characterize a material microstructure. There exist several approximation schemes for $I^{(i)}(\mathbf{x})$ (i..e, the material microstructure), including the Gaussian random field (GRF) models [30] and reduced-order representation [31]. The key idea involved in these approximation schemes is to reduce the large number of degrees of freedom required to specify unnecessary structural details to a small set of parameters or data points that statistically characterize the material microstructure for purpose of modeling and visualization. However, the physical significance associated with these parameters is usually not obvious. On the other hand, as we will show in the ensuing sections, the parameters involved in the correlation functions such as the "correlation length" often have clear physical meaning and directly correspond to a salient structural feature of the material.

Two-point correlation function

Given the indictor function $I^{(i)}(\mathbf{x})$, the volume fraction of phase i is then given by

$$\phi_i = < I^{(i)}(\mathbf{x}) > \tag{2}$$

where <> denotes the ensemble average over many independent material samples or volume average over a single large sample if it is spatially "ergodic" [3]. The two-point correlation function $S_2^{(ij)}(\mathbf{x}_1, \mathbf{x}_2)$ associated with phases i and j is defined as

$$S_2^{(ij)}(\mathbf{x}_1, \mathbf{x}_2) = < I^{(i)}(\mathbf{x}_1) I^{(j)}(\mathbf{x}_2) > \tag{3}$$

which also gives the probability that two randomly selected points $\boldsymbol{x}_1$ and $\boldsymbol{x}_2$ fall into phase i and j respectively (see Figure 2). For a material with q distinct phases, there are totally q^*q different S_2. However, it has been shown that only q of them are independent [3,32] and the remaining $q^*(q\text{-}1)$ functions can be explicitly expressed in terms of the q independent ones.

For statistically homogeneous materials as the examples considered here, there is no preferred center in the microstructure. Therefore, the associated S_2 depends only on the relative vector displacement between the two points [3], i.e.,

$$S_2(\mathbf{x}_1, \mathbf{x}_2) = S_2(\mathbf{x}_2 - \mathbf{x}_1) = S_2(\mathbf{r}) \tag{4}$$

where $\boldsymbol{r} = \boldsymbol{x}_2 - \boldsymbol{x}_1$. At $\boldsymbol{r} = 0$ the auto-correlation function gives the probability that a randomly selected point falls into the phase of interest, i.e., the volume fraction of the associated phase. On the other hand, the cross correlation function is zero at $\boldsymbol{r} = 0$, since the probability of finding a single point falling into two different phases is zero. At large $\boldsymbol{r}$ values, the probabilities of finding the two points in the phases of interest are independent of one another, leading to ϕ_i^2 for the auto-correlation

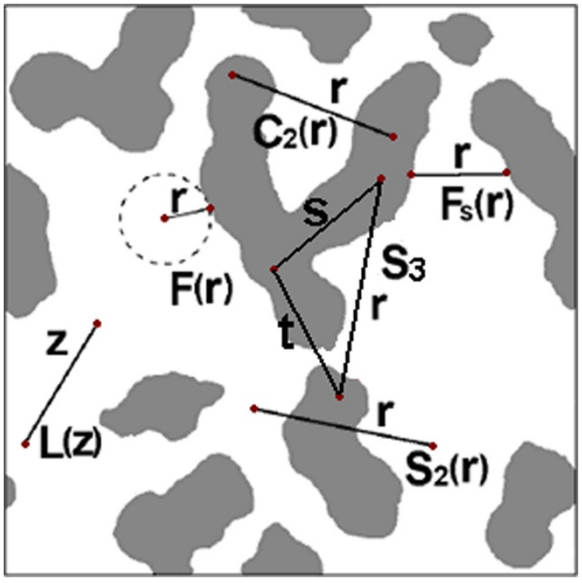

Figure 2 Schematic illustration of the probability interpretation of the correlation functions. The 2-and 3-point configurations (i.e., line segments and triangle) shown represent the events contributing to the associated correlation functions.

functions and $\phi_i\phi_j$ for the cross correlation function. For a statistically isotropic material, S_2 depends only on the scalar distance between a pair of points.

We note that the general n-point correlation function S_n which gives the probability of finding a particular n-point configuration in specific phases can be defined in a similar manner as S_2; see Eq. (2). It has been shown that the effective properties of a heterogeneous material can be explicitly expressed as series expansions involving certain integrals of S_n. Interested readers are referred to Ref. [3] for detailed discussions of S_n and their properties.

Lineal-path function

The lineal-path function $L^{(i)}(\boldsymbol{r})$ gives probability that a randomly selected line segment of length $r = |\boldsymbol{r}|$ along the direction of vector $\boldsymbol{r}$ entirely falls into phase i (see Figure 2) [33,34]. At $\boldsymbol{r} = 0$, $L^{(i)}(0)$ reduces to the probability of finding a point in phase i and thus, $L^{(i)}(0) = \phi_i$. In materials that do not contain system-spanning clusters, the chance of finding a line segment with very large length entirely falling into any phases is vanishingly small. Accordingly, for large $\boldsymbol{r}$ values $L^{(i)}$ decays to zero rapidly in such materials. The lineal-path function contains partial topological connectedness information of the material's phases, i.e., that along a lineal-path. Generally, the lineal-path function underestimates the degree of clustering in the system (e.g., two points belonging to the same cluster but not along a specific lineal path will not contribute to L).

Two-point cluster function

The two-point cluster correlation function $C_2^{(i)}(\mathbf{x}_1, \mathbf{x}_2)$ gives the probability that two randomly selected points $\boldsymbol{x}_1$ and $\boldsymbol{x}_2$ fall into the same cluster of phase i (see Figure 2) [35,36]. For statistically homogeneous materials, C_2 depends only on the relative vector displacement between the two points, i.e., $C_2(\mathbf{x}_1, \mathbf{x}_2) = C_2(\mathbf{r})$. In contrast to the lineal-path function, C_2 contains complete clustering information of the phases, which has been

shown to have dramatic effects on the material's physical properties [3]. Moreover, unlike S_2 and L, the cluster functions generally cannot be obtained from lower-dimensional cuts (e.g., 2D slices) of a 3D microstructure, which may not contain correct connectedness information of the actual 3D system.

It has been shown that C_2 is related to S_2 via the following equation [35]

$$S_2^{(ii)}(\mathbf{r}) = C_2^{(i)}(\mathbf{r}) + D_2^{(i)}(\mathbf{r}) \tag{5}$$

where $D_2^{(i)}(\mathbf{r})$ measures the probability that two points separated by $\boldsymbol{r}$ fall into different clusters of the phase of interest. In other words, C_2 is the connectedness contribution to the standard two-point correlation function S_2. For microstructures with well-defined inclusion, C_2 (r) of the inclusions is a short-ranged function that rapidly decays to zero as r approaches the largest linear size of the inclusions. We note that although C_2 is a "two-point" quantity, it has been shown to embody higher-order structural information which makes it a highly sensitive statistical descriptor over and above S_2 [24].

Other correlation functions

Other types of correlation functions include the surface functions and pore-size function. The surface correlation functions F_s [3,37] are associated with the probability of finding an n-point configuration with a subset of points falling on to the surface, while the others lie in the bulk of the phase of interest. Specifically, the surface-surface correlation function $F_{ss}(r)$ can be considered as the probability of finding two points separated by r, which both fall into a dilated region associated with the surface of one phase in the limit of vanishingly small dilation. The surface-void correlation function $F_{sv}(r)$ is the probability of finding two points separated by r, one in the phase of interest ("void") and the other in a dilated region associated with the surface of one phase in the limit of vanishingly small dilation. The pore-size function F [38,39] provides statistics of the size of the largest spherical region centered at a randomly selected point in the phase of interest that entirely lie in this phase. Figure 2 schematically illustrates the probability interpretation of the aforementioned statistical microstructural descriptors by depicting the events that contribute to the correlation functions.

Modeling microstructure via correlation functions

It is rigorously shown that a heterogeneous microstructure can be uniquely determined given the complete set of n-point correlation functions S_n. In practice, such a complete set is generally not available and is not suitable for microstructure modeling due the complexity involved in computing these quantities from experimental images. As we mentioned above, the non-traditional functions such as the lineal-path function L and the cluster function C_2 contain topologically connectedness information that is only embodied in higher-order S_n. Therefore, we expect that a carefully selected set of aforementioned lower-order correlation functions (e.g., S_2, C_2, L, F_{ss}, F_{sv}, F, etc.), which capture different structural features such as connectivity and surface of the material system, could provide a statistically accurate characterization of the microstructure. In other words, a microstructure $\boldsymbol{M}$ can be modeled and represented as a set of selected lower-order correlation functions, i.e.,

$$M = \{S_2, C_2, L, F_{ss}, F_{sv}, F, \ldots\} \tag{6}$$

Methods

A variety of reconstruction schemes have been developed that enable one to generate material microstructure models from limited structural information. Examples of such schemes include the Gaussian random field method [30], phase recovery method [40], multi-point reconstruction method [41], and raster-path method [42]. The Gaussian random field method [30] was originally devised to reconstruct realizations of statistically homogeneous and isotropic random media from the associated two-point correlation functions. The phase recovery method enables one to take into account the full vector information contained in the two-point statistics associated with the material, and thus allows the reconstructions of complex anisotropic microstructure and polycrystalline materials [40]. The multi-point reconstruction method was originally developed for the reconstruction of porous geomaterials from 2D images [41]. Instead of using two-point statistics associated with the entire 2D microstructure, this method incorporates all n-point statistics within a smaller window containing a portion of the microstructure. The recently developed raster-path method allows one to employ the multi-point statistics in a much more efficient way [42]. Specifically, instead of extracting the statistics from the 2D microstructure, a cross-correlation function is introduced to directly compare a reconstructed portion of the material to the target 2D image.

All of the aforementioned reconstruction methods have been successfully applied to model certain classes of materials. However, they all require specific correlation functions or image data as input information. Another widely-used reconstruction method is the stochastic optimization procedure devised by Yeong and Torquato [25,26]. The Yeong-Torquato (YT) procedure enables one to incorporate an arbitrary number of correlation functions of any type into the reconstructions. Specifically, a trial microstructure is evolved using simulated annealing procedure such that the set of correlation functions sampled from the trial microstructure match the set of target statistics up to a prescribed small tolerance (see below for algorithmic details). Its flexibility of incorporating arbitrary correlation functions into the reconstruction makes the YT procedure an ideal protocol to examine the information content of different statistical descriptors associated with a material system and select the most sensitive descriptors for microstructure modeling. Therefore, we will employ the YT procedure in our study. However, due to its stochastic nature a large number of intermediate trial microstructures need to be generated and analyzed, which makes it computationally intensive. Several different implementations of the Y-T procedure have been devised to improve it efficiency [22-24,43,44].

Yeong-Torquato reconstruction procedure

We use the Yeong-Torquato (YT) reconstruction procedure [25,26] to generate virtual 3D microstructures from a specific set of correlation functions discussed in the previous Statistical microstructural descriptors. In the YT procedure, the reconstruction problem is formulated as an "energy" minimization problem, with the energy functional E defined as follows

$$E = \sum_{\alpha} \sum_{r} \left[f^{\alpha}(r) - \overline{f^{\alpha}}(r) \right]^2 \tag{7}$$

where $\overline{f^{\alpha}}(r)$ is a target correlation function of type α and $f^{\alpha}(r)$ is the corresponding function associated with a trial microstructure. The simulated annealing method [45] is

usually employed to solve the aforementioned minimization problem. Specifically, starting from an initial trial microstructure (i.e., *old* microstructure) which contains a fixed number of voxels for each phase consistent with the volume fraction of that phase, two randomly selected voxels associated with different phases are exchanged to generate a *new* trial microstructure. Relevant correlation functions are sampled from the new trial microstructure and the associated energy is evaluated, which determines whether the new trial microstructure should be accepted or not via the probability:

$$p_{acc}(old \rightarrow new) = \min\left\{1, \exp\left(\frac{E_{old}}{T}\right) / \exp\left(\frac{E_{new}}{T}\right)\right\} \tag{8}$$

where T is a virtual temperature that is chosen to be initially high and slowly decreases according to a cooling schedule [23]. Initially, T is chosen to be high in order to allow a sufficiently large number of "up-hill" (energy increasing) trial microstructures. As T gradually decreases, the "up-hill" moves become less favorable. This significantly decreases the chances that the final microstructure gets stuck in a shallow local energy minimum, as illustrated in Figure 3. In practice, it is usually extremely difficult for the system to converge to the global minimum. Thus, the annealing process is considered complete if E is smaller than a prescribed tolerance, which we choose to be 10^{-10} here.

Efficient sampling method for correlation functions

The probabilistic interpretations of the correlation functions discussed in Statistical microstructural descriptors enable us to develop a general sampling method for reconstruction of statistically homogeneous and isotropic materials based on the "lattice-gas" formalism [22-24]. In this formalism, pixels with different values (occupying the lattice sites) correspond to distinct local states and pixels with the same value are considered to be "molecules" of the same "gas" species. The correlation functions of interest can be obtained by binning the separation distances between the selected pairs of molecules from particular species.

In the case of S_2, all molecules are of the same species. We denote the number of lattice-site separation distances of length r by $N_S(r)$ and the number of molecule-pair separation distances of length r by $N_P(r)$. Thus, the fraction of pair distances with both ends occupied by the phase of interest, i.e., the two-point correlation function, is given by $S_2(r) = N_P(r)/N_S(r)$. To obtain C_2, one needs to partition the molecules into different subsets Γ_i (species) such that any two molecules of the same species are connected by a path composed of the same kind of molecules, i.e., molecules that form a cluster, which

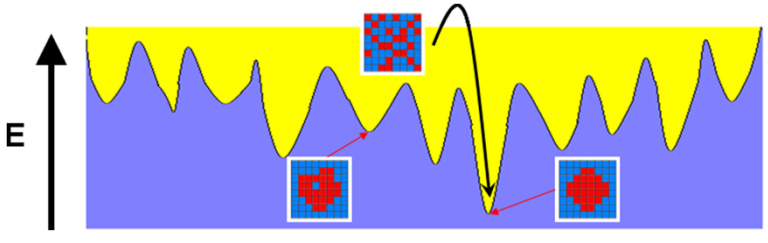

Figure 3 Schematic illustration of the simulated annealing procedure. The acceptance of energy-increasing trial microstructure allows the system to escape from local energy minima and thus, increases the probability of convergence to the global minimum.

is identified using the "burning" algorithm [24]. The number of pair distances of length r between the molecules within the same subset Γ_i is denoted by $N_P^i(r)$. The two-point cluster function is then given by $C_2(r) = i\ N_P^i(r)/N_S(r)$. The calculation of F_{SS} and F_{SV} requires partitioning the molecules into two subsets: the surface set K_S containing only the molecules on the surfaces of the clusters and the volume set K_V containing the rest. In a digitized medium, the interface necessarily has a small but finite thickness determined by the pixel size. Thus, the surface–surface and surface–void correlation functions can be regarded as probabilities that are given by $F_{SS} = N_{SS}(r)/N_S(r)$ and $F_{SV} = N_{SV}(r)/N_S(r)$, respectively; where $N_{SS}(r)$ gives the number of distances between two surface molecules with length r and N_{SV} is the counterpart for pairs with one molecule on the surface and the other inside the cluster.

The lineal path function L can be obtained by computing the lengths of all digitized line segments (chords) composed of pixels of the phase of interest, and for each chord incrementing the counters associated with the distances equal to and less than that chord length [24]. The chord-length density function p can then be easily obtained by binning the chord lengths that are used to compute L. The pore-size function F can be computed by finding the minimal separation distances of pixels within the phase of interest to those at the two-phase interfaces. The minimal distances are then binned to obtain a probability distribution function, the complementary cumulative distribution function of which is the pore-size function F [24].

Efficient method for re-computing correlation functions for trial microstructures

Generally, several hundred thousand trials need to be made to achieve such a small tolerance. Therefore, efficient sampling methods [22-24] are used that enable one to rapidly obtain the prescribed correlation functions of a new microstructure by updating the corresponding functions associated with the old microstructure, instead of completely re-computing the functions. Specifically, a distance matrix $\boldsymbol{D}$ that stores the separation distances of all "molecule" pairs is established when the system is initialized and the molecules are partitioned into different "species" depending on their positions, as discussed in the main article. The quantities N_P, N_P^i, N_{SS} and N_{SV} (all defined in the previous subsection) can be obtained by binning the separation distances of selected pairs of molecules from particular species. Recall that the molecules are pixels associated with different values indicating the species, i.e., the clusters or the surface/volume set they belong to.

In the reconstruction procedure, a trial microstructure is generated by moving a randomly selected pixel of the phase of interest to an unoccupied site. This results in changes of the separation distances between the moved the pixel and all of the other pixels, and causes two kinds of possible species events. The first kind is a "cluster" event, which involves breaking and combining clusters. For example, if the selected pixel happens to be a "bridge" connecting several sub-clusters, removing the bridge will make the original single cluster break into smaller pieces, i.e., new species (clusters) are generated. Similarly, the reverse of the above process can occur, i.e., a randomly selected pixel moved to a position where it connects several small clusters to form a larger cluster, which leads to combination of clusters and annihilation of species. The other kind of species event is the transition of pixels between surface and

volume sets. If a pixel originally on the surface is removed, certain volume pixels (i.e., those inside the phase of interest) will now constitute the new surface and vice versa. The selected pixel itself could also undergo such a transition, depending on its original and new positions, e.g., a volume pixel originally inside the phase of interest could be moved to the interface to become a surface pixel.

The contributions of the number of pair distances to N_{P}, N_{P}^{i}, N_{SS} and N_{SV} from the pixels in old microstructure involved in the species events are computed and subtracted accordingly. The new contributions can be obtained by binning the separation distances of pixel pairs in the new microstructure involved in the species event, which are then added to the corresponding quantities N_{P}, N_{P}^{i}, N_{SS} and N_{SV}. This method only requires operations on a small number of pixels, including retrieving and binning their separation distances and updating the species sets (i.e., the clusters and surface/volume set). The use of the distance matrix $\boldsymbol{D}$ speeds up the operations involving distances. However, for very large systems (e.g., those including millions of pixels), storing $\boldsymbol{D}$ requires very a large amount of computer memory. An alternative is to re-compute the separation distances of the pixel pairs involved in the species events for every trial microstructure, instead of explicitly storing all the distances in $\boldsymbol{D}$. This may slightly slow down the reconstruction process but make it easy to handle very large systems. Correlation functions of the new microstructure can then be obtained from the updated N_{P}, N_{P}^{i}, N_{SS} and N_{SV} (i.e., dividing those quantities by N_{S}). Importantly, the complexity of the algorithm is linear in the total number of pixels (molecules) within the system.

Results

In this section, we apply the aforementioned statistical descriptors and stochastic reconstruction techniques to model several material systems including an anisotropic aluminum alloy, a polycrystalline tin solder and the structural evolution in an isothermally-aged binary lead-tin alloy. Moreover, we examine the information content of different correlation functions by studying a model material microstructure consisting of equal-sized hard spheres in a matrix.

Inclusion distribution anisotropy in rolled aluminum alloy

Aluminum (Al) alloys have been widely used in many engineering structures especially in automotive and aircraft applications due to their unique high strength-to-weight ratio and corrosion resistance. An aluminum alloy almost always has secondary phase inclusions and particles with impurities that are present in the microstructure. Due to rolling of the alloy, the inclusions usually possess an anisotropic distribution, with the dimension along the rolling direction being significantly elongated. This in turn results in an overall anisotropic alloy microstructure.

In order to model an alloy microstructure with anisotropic Fe-rich and Si-rich inclusions in Al matrix, we will use correlation functions along three orthogonal directions, i.e., the longitudinal or rolling (L), transverse (T) and short transverse (S) directions [46]. Specifically, we denote the directional two-point correlation function, two-point cluster function and lineal-path function of type α along direction β respectively by $S_2^{\alpha,\beta}(r)$, $C_2^{\alpha,\beta}(r)$ and $L^{\alpha,\beta}(r)$ where α = {Fe, Si, Fe-Si} and β = {L, T, S}.

Accordingly, in order to obtain these functions from a digitized microstructure, only the "molecules" along specific directions are considered (see Results).

The directional two-point correlation function of the inclusion phase α can be approximated with the following function:

$$S_2^{\alpha,\beta}(r) = \left\{\phi_\alpha\left[A_\beta^\alpha \exp\left(B_\beta^\alpha \cdot r\right) + \left(1-A_\beta^\alpha\right)V_{\text{int}}\left(r;\bar{D}_\beta^\alpha\right)\right] + \phi_\alpha^2\left[1-V_{\text{int}}\left(r;\bar{D}_\beta^\alpha\right)\right]\right\}\Theta\left(\bar{D}_\beta^\alpha - r\right) + \phi_\alpha^2\Theta\left(r-\bar{D}_\beta^\alpha\right) \tag{9}$$

where ϕ_α is the volume fraction, A_β^α, B_β^α and $\bar{D}_\beta^\alpha$ are parameters to be determined. The approximation (9) includes two "basis" functions: the Debye random medium function $\exp(Br)$ [22,47] and $V_{\text{int}}(r; D)$ [3], which is the scaled intersection volume of two isotropic inclusions with linear size D separated by r:

$$V_{\text{int}}(r;D) = 1 - \frac{3r}{2D} + \frac{r^3}{2D^3} \tag{10}$$

and $\Theta(x)$ is the Heaviside function, i.e.,

$$\Theta(x) = \begin{cases} 1 & x \geq 0 \\ 0 & x < 0 \end{cases} \tag{11}$$

In other words, one can consider the alloy microstructure as a mixture of "clusters of all shape sizes" (features of a Debye random medium) and well defined inclusions (characterized by V_{int}). For the anisotropic inclusions, we consider that each direction possesses distinct combination parameter A_β^α, correlation parameter B_β^α and effective size $\bar{D}_\beta^\alpha$, which is the effective linear size or "length" of the inclusions along that direction. The values of these parameters are determined such that the approximated functions best match the actual autocorrelation function (i.e., the squared difference between two functions is minimized). In Tables 1 and 2, we provide the values of the parameters for the Fe-rich and Si-rich inclusions in the alloy, respectively. Note that we do not model the cross-correlation function S_2^{Fe-Si} since in the low φ limit its values are several orders of magnitude smaller than the autocorrelation functions, which again suggests that there are no significant inter-particle spatial correlations.

By definition, the two-point cluster function C_2 measures the contributions from the point pairs in the same cluster (inclusion) in S_2; see Eq. (5). Thus, we approximate C_2 of the inclusion phase α as follows:

$$C_2^{\alpha,\beta}(r) = \phi_\alpha\left[A_\beta^\alpha \exp\left(B_\beta^\alpha \cdot r\right) + \left(1-A_\beta^\alpha\right)\left(1 - \frac{3r}{2\bar{D}_\beta^\alpha} + \frac{r^3}{2\bar{D}_\beta^\alpha}\right)\right]\Theta\left(\bar{D}_\beta^\alpha - r\right) \tag{12}$$

Table 1 The values of A_β^α, B_β^α and $\bar{D}_\beta^\alpha$ for the Fe-rich inclusions along three orthogonal directions in the alloy

Fe-rich inclusions	Longitudinal	Transverse	Short transverse
A_β^α	0.801	0.850	0.902
B_β^α	−0.350	−0.504	−0.579
$\bar{D}_\beta^\alpha$	81.2	32.0	18.9

Table 2 The values of A_β^α, B_β^α and $\bar{D}_\beta^\alpha$ for the Si-rich inclusions along three orthogonal directions in the alloy

Si-rich inclusions	Longitudinal	Transverse	Short transverse
A_β^α	0.918	0.898	0.951
B_β^α	−0.480	−0.548	−0.679
$\bar{D}_\beta^\alpha$	86.8	25.9	11.0

where the parameters A_β^α, B_β^α and $\bar{D}_\beta^\alpha$ are given in Tables 1 and 2 respectively for the Fe-rich and Si-rich inclusions.

The YT stochastic reconstruction procedure is employed to generate virtual alloy microstructures from the associated S_2 [Eq. (9)] and C_2 [Eq. (12)]; see Figure 4. By quantitatively comparing the experimentally obtained structure and the reconstructions via the lineal-path functions of the inclusion phases, it can be clearly seen that the combination of S_2 and C_2 is sufficient to statistically characterize the microstructure, i.e., the complex alloy microstructure can be modeled by six directional correlation functions with closed analytical forms, which only depend on the parameters given in Tables 1 and 2. In other words, the large 3D microstructural array specifying the local state of each individual voxels can be reduced to a handful of scalar parameters that statistically model the alloy microstructure.

Polycrystalline tin solder

Tin has been widely used as solider materials in electronic packaging. Due to heterogeneous cooling and the existence of intermetallic particles, a tin solder joint usually processes a polycrystalline microstructure. The mechanical properties of the joint are largely determined by the grain size, orientation and the degree of mis-orientation between the grains. Such structural information can be obtained via electron back scattered diffraction (EBSD) experiments (see Figure 5A). However, the EBSD image technique only allows

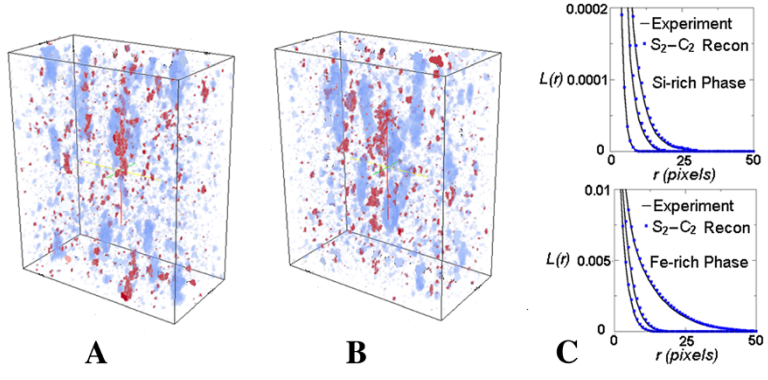

Figure 4 Modeling anisotropic aluminum alloy using directional correlation functions S_2 and C_2. **(A)** Actual microstructure as obtained from x-ray tomographic microscopy. Fe-rich phase is shown in blue and Si-rich phase is shown in red. **(B)** Stochastically reconstructed microstructure that reproduces the salient features of the actual microstructure. **(C)** Comparison of the lineal-path functions associated with the Fe-rich and Si-rich phases in the actual and reconstructed microstructures. The dimensions of the alloy microstructure are 180 μm *340 μm *430 μm. The unit of length used in the figures is the edge length of a pixel, which is roughly 1.8 μm.

one to probe the surface of the material sample. Therefore, serial sectioning is required to acquire successive 2D images at different depth of the polycrystalline structure. A final reconstruction can be obtained by carefully stacking these 2D images [20,21].

Our modeling procedure provides an alternative approach to generate virtual 3D polycrystalline structure models from single or a few EBSD images of the material surface. Specifically, the colored EBSD image, in which different colors represent different grain orientations, is first converted to a gray-scale image. Then the gray-scale image is thresholded to generate a multiphase material structure such that each phase corresponds to a narrow range of gray values (i.e., a narrow distribution of orientation). The morphology of each phase includes compact regions that are associated the grains of different orientations (i.e., colors in the original EBSD image). The two-point correlation functions S_2 associated with the individual phases are computed (see Figure 5B). Under the assumption that the structure is statistically homogeneous and isotropic, the sampled S_2 from 2D images are representative of the full 3D microstructure and thus, can be used to generate 3D reconstructions. Similarly, the surface-surface correlation functions $F_{SS}(r)$ sampled from the 2D images incorporate 3D structural information for statistically homogeneous and isotropic systems, and thus, can also be employed to render virtual 3D microstructures.

Figure 5C and D respectively shows the reconstructed 3D polycrystalline structures using S_2 alone and using the combination of S_2 and $F_{SS}(r)$. Both reconstructions statistically reproduce the key structural features including the size and shape of the grains and the

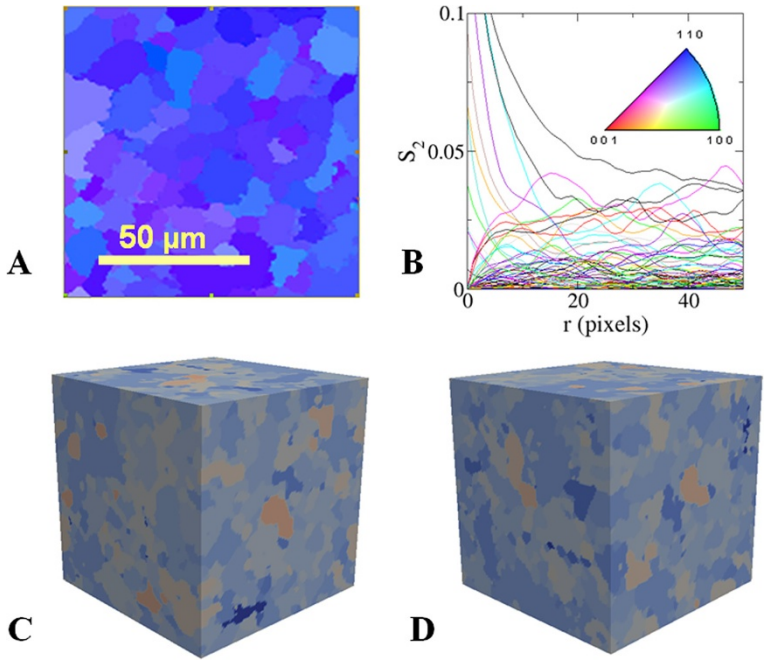

Figure 5 Modeling a polycrystalline tin solder as a multiphase material using the two-point correlation function obtained from a 2D EBSD image. (A) The 2D EBSD image of the surface of the solder. **(B)** The associated two-point correlation functions of the phases and cross correlation functions. Inset: The crystallographic triangle providing the orientations of the grains shown in **(A)**. **(C)** A 3D reconstruction using two-point correlation functions S_2. **(D)** A 3D reconstruction using the surface correlation function F_{SS} in addition to the two-point correlation functions. The linear size of the system we considered is 85 μm and one pixel = 0.6 μm.

orientation correlation between neighboring grains, as can be seen by comparing the surfaces of the 3D virtual microstructures to the target 2D image. Quantitative comparison between the reconstructions (not shown here) indicates that incorporating the surface function does not lead to additional improvement of the accuracy of the reconstruction. This suggests that S_2 alone would be sufficient to model this polycrystalline system. We emphasize that a quantitative comparison between the reconstructions and experimentally obtained 3D structure is necessary to definitely ascertain the accuracy of the reconstructions. However, the latter is currently not available.

Structural evolution in lead-tin binary alloy

Binary lead/tin alloys have been widely used as solders [48]. In particular, a eutectic alloy of 63% tin (Sn), 37% lead (Pb) has been used as interconnect due to its unique low melting point (183°C), good wettability, and excellent mechanical properties. The eutectic alloy microstructure contains a Pb-rich phase and a Sn-rich phase, which can possess both laminar and globular morphologies. The salient microstructural features such as the width and extent of the laminar phases as well as the size and spatial distribution of the globular phases can significantly affect the overall mechanical properties of the alloy. At temperatures below the eutectic melting point, the enhanced diffusion of Pb and Sn atoms can lead to significant coarsening in the alloy, which lowers the total interfacial energy [49]. A heat treatment (e.g, annealing) can then be employed to "tune" the eutectic microstructure to achieve desirable material performance. The rate of coarsening increases with temperature and it is of particular importance to quantitatively model and predict the degree of coarsening in the design of materials for high temperature applications.

Figure 6 demonstrates our modeling of the structural evolution in a binary alloy (Pb37Sn63) annealed at 175°C up to 216 h [29], which can be accurately characterized by the associated time-dependent scaled two-point correlation functions $f(r)$, i.e.,

$$f(r) = \frac{S_2(r) - \phi^2}{\phi(1-\phi)} \tag{13}$$

Using phase-field modeling, we have found that a growing length scale λ characterizing the coarsening process can be defined from the correlation length (i.e., a scalar parameter) in $f(r)$ associated with microstructures annealed for different amounts of time. 2D optical images of polished surface of the sample were taken at different annealing times (see the upper panels of Figure 6) and careful measurements of λ from these images have shown that λ satisfies the scaling relation $\lambda(t) \sim t^{1/3}$, which is consistent with the phase-field modeling results and expected for systems that are diffusion-controlled. This allows us to construct a universal functional form of $f(r)$ parameterized by $\lambda(t)$ to statistically characterize the entire spectrum of microstructures undergone coarsening, i.e.,

$$f(r) = \exp(-ar/\lambda)\cos(\pi r/\lambda + b)/\cos(b) \tag{14}$$

where $a = 3.5$ and $b = 0.6$ are parameters depending on the initial microstructure but not the annealing time. Snapshots of evolving alloy microstructure at specific annealing times reconstructed from the correlation function f [$\lambda(t)$] are shown in the middle

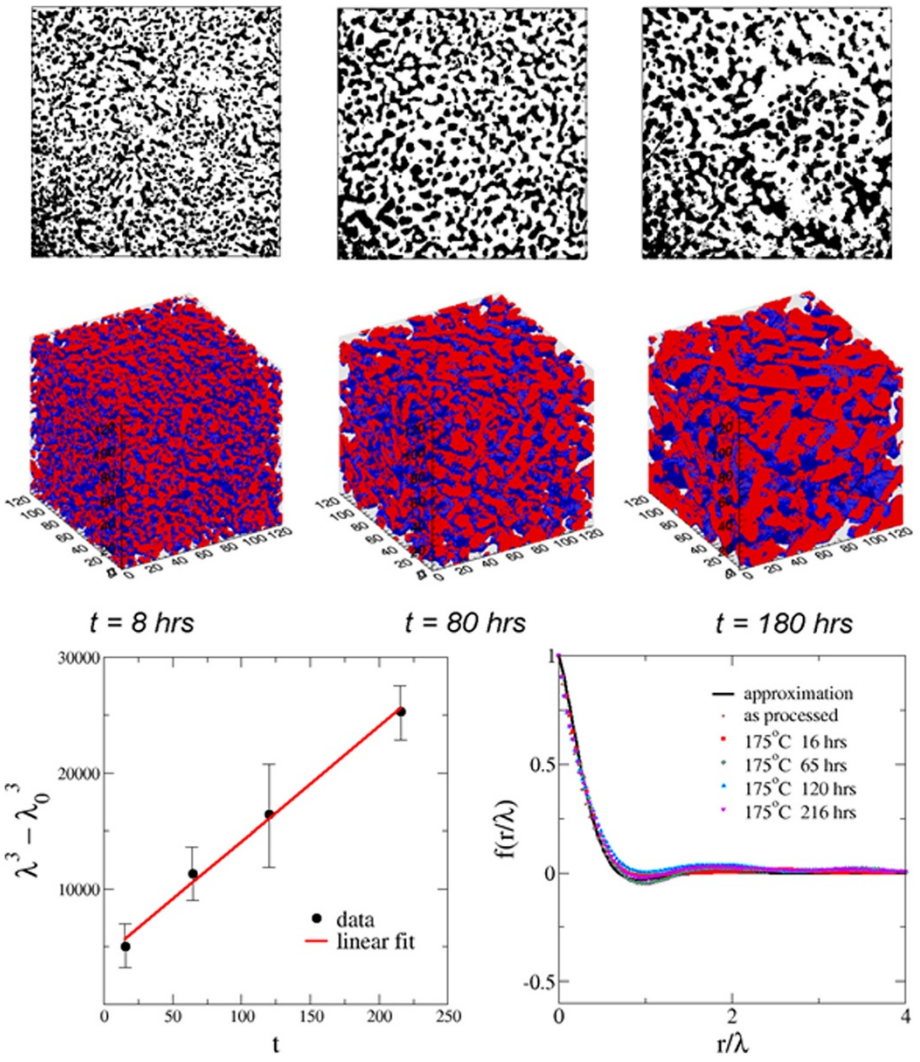

Figure 6 Modeling the structural evolution of a binary lead/tin alloy. Upper panels: 2D optical images of polished alloy surface at different annealing times (lead-rich phase is shown in black). The linear size of the system is roughly 200 μm. Middle panels: Predicted microstructures of lead/tin alloy aged for different times (lead-rich phase is shown in red with blue surfaces). The linear size of the system is roughly 80 μm. The unit of length used in the plots is the edge length of a pixel, which is roughly 0.625 μm. Lower left panel: A quantitatively measured growing length scale charactering the coarsening process. Lower right panel: The universal functional form of the scaled correlation functions. The unit of time is hour.

panels of Figure 6. The development of coarsening in the microstructure is clearly seen. The lower panels of Figure 6 show the universal function on to which the scaled f associated with experimentally obtained microstructures annealed at different times collapse. The quantitative relation between the material microstructure as represented by the correlation function $f[\lambda(t)]$ and the processing-condition parameter t lies the mathematical foundation for material design and optimization. In particular, this procedure of 4D material microstructure modeling allows one to directly and quantitatively tie processing parameters (e.g., the annealing time t in this case) to the microstructure. Subsequent analysis and simulations on the physical properties and performance can be carried out to further establish the processing-structure-performance relations.

Hard-sphere packing

Finally, we employ the procedure to examine the information content of different correlation functions associated with a hard-sphere packing, i.e., a dispersion of hard spheres in a matrix [24]. This structure has been widely used in models for particle-reinforced composites, colloids, and granular materials. The packing shown in Figure 7A is generated using the standard Metropolis Monte Carlo technique for a canonical ensemble of hard spheres in a cubical box under periodic boundary conditions. The three reconstructions shown in Figure 7B-D are generated respectively using S_2 alone, the combination of S_2 and the pore-size function F, and the combination of S_2 and the cluster function C_2. A visual comparison of the reconstruction involving C_2 reveals that it accurately yields a dispersion of well-defined spherical inclusions of the same size, in contrast to the S_2 reconstruction, which grossly overestimates clustering of the "sphere" phase. In addition, although the reconstruction incorporating F provides improvement over the rendition of the S_2-alone reconstruction, it is still inferior to the S_2–C_2 reconstruction in reproducing both the size and shape of the "sphere" phase. The accuracy of the reconstructions can also be quantitatively ascertained by comparing the lineal-path function associated with the sphere phase in the rendered microstructures, as shown in Figure 7E. This example clearly illustrates the utility of our procedure in examining the information content of various statistical descriptors for structural characterization. In the sphere-packing system, the combination of S_2 and C_2 provide a sensitive descriptor of the structure, suggesting that similar material systems (e.g., particle reinforced composites) can be accurately modeled by these quantities.

Discussion and conclusion

In this paper, we presented a framework to model the microstructure of complex heterogeneous materials via certain lower-order correlation functions associated

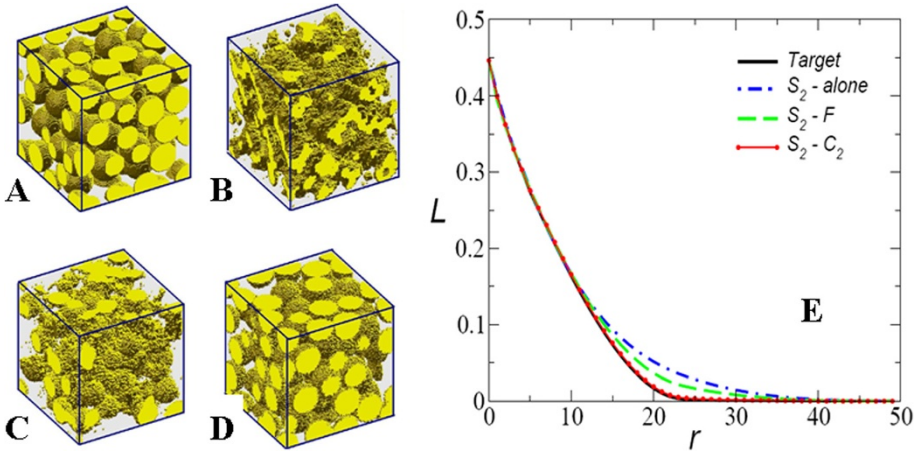

Figure 7 Reconstructions of a model microstructure with spherical inclusions dispersed in a matrix (A) respectively from the standard two-point correlation function S2 (B), the pore-size function F (C) and the two-point cluster function C2 (D). The quality of the reconstructions is clearly improved by successively incorporating clustering information, verified by quantitative comparisons of the lineal-path functions L of the target and the reconstructions **(E)**. The unit of the length in the figure is the edge length of a pixel, which is 1 μm. The linear size of the system is 128 μm. The diameter of the spheres is 25 μm.

with the material's phases. Such correlation functions quantitatively characterize various topological and geometrical features of the material microstructure and play an important role in the quantitative connection between the material microstructure and the effective physical properties as obtained via homogenization theories. Representing a microstructure with the combination of a selected set of correlation functions allows one to reduce the large data sets for a complete specification of all of the local states in a microstructure to a handful of simple scalar functions that statistically capture the salient structural features of the material. Given a specific set of correlation functions, the Yeong-Torquato reconstruction procedure can be employed to generate 3D virtual microstructure models compatible with the functions. Moreover, the Y-T procedure also allows one to examine the information content of different correlation functions by quantitatively comparing the reconstructions to the actual microstructure in order to determine the set of most sensitive morphological descriptors for such a class of materials for microstructure modeling and virtual material generation. The accuracy of the reconstruction can be quantitatively ascertained by comparing statistical descriptors (e.g., various correlation function, distribution of cluster size, continuity etc.) that are not constrained in the optimization.

To demonstrate its utility, we employed the framework to model a variety of material systems, including an aluminum alloy with anisotropic secondary phases, a polycrystalline tin solder, the structural evolution in binary lead-tin alloy when aged, and a model microstructure with hard spheres dispersed in a matrix. We found that for certain materials, such as the lead-tin alloy, the standard two-point correlation function S_2 alone is sufficient to provide a statistically accurate characterization of the associated microstructure. On the other hand, a realistic reconstruction of the hard-sphere packing model clearly requires additional topological connectedness information as contained in the cluster function C_2. In general, we expect that successively incorporating additional morphological information by increasing the number of correlation functions as input for the Y-T procedure would lead to more and more accurate reconstructions. In practice, a set of carefully chosen correlation functions sensitive to the key structure features would be sufficient for characterizing and modeling a material of interest. We also note that for certain microstructures such as percolated thin filaments, topological transformations (e.g., dilation and erosion) could be used to further improve the accuracy of the reconstruction [50].

Our framework enables one to model structural evolution over time via time-dependent correlation functions. Physics-based models (e.g., the phase-field modeling in the case of the lead-tin alloy example shown here) can be employed to suggest growing length scale or other key structural parameters that are directly manifested in the correlation function modeling the material structure. A quantitative relation between the processing condition and the structural evolution is established by incorporating the key processing parameters such as annealing temperature and annealing time into the associated correlation functions. Such relations are crucial to the integrated design of optimal multifunctional materials. Besides examining the information content of correlation functions, the stochastic reconstruction procedure can be adapted to investigate other types of structure data, such as limited-angle tomography projections. Understanding the information content of tomography data could lead to significant reduction of the number of projections acquired to characterize a single microstructure and thus, improve the efficiency for 4D characterization using tomography.

Availaiblity of supporting data

The C++ program for the stochastic reconstruction described in the paper is available upon request.

Competing interests
The authors declare no competing interests.

Authors' contributions
YJ and NC contributed equally to this article. Both authors read and approved the final manuscript.

Authors' information
Revised version submitted to:
Integrating Materials and Manufacturing Innovation
January, 2014

Acknowledgements
This work was supported by the Division of Materials Research at National Science Foundation under award No. DMR-1305119. The authors acknowledge A. Kirubanandham for the EBSD images of pure Sn. Y. J. also thanks Arizona State University for the generous start-up package.

Received: 5 November 2013 Accepted: 30 January 2014
Published: 4 March 2014

References

1. Christensen RM (1979) Mechanics of Composite Materials. Wiley, New York, 1979
2. Nemat-Nasser SM, Hori M (1999) Micromechanics: Overall Properties of Heterogeneous Solids. Elsevier Science Publishers, Amsterdam
3. Torquato S (2002) Random Heterogeneous Materials: Microstructure and Macroscopic Properties. Springer, New York
4. Sahimi M (2003) Heterogeneous Materials I: Linear Transport and Optical Properties, and II: Nonlinear and Breakdown Properties and Atomistic Modeling. Springer, New York
5. Millar DIA (2012) Energetic Materials at Extreme Conditions. Springer Ph.D. Thesis, New York
6. Haymes RC (1971) Introduction to Space Science. John Wiley and Sons Inc, New York, NY, 1971
7. Thornton K, Poulsen HF (2008) Three-dimensional materials science: an intersection of three-dimensional reconstructions and simulations. MRS Bull 33:587
8. Brandon D, Kaplan WD (1999) Microstructural Characterization of Materials. John Wiley & Sons, New York
9. Baruchel J, Bleuet P, Bravin A, Coan P, Lima E, Madsen A, Ludwig W, Pernot P, Susini J (2008) Advances in synchrotron hard x-ray based imaging. C R Physique 9:624
10. Kinney JH, Nichols MC (1992) X-ray tomographic microscopy (XTM) using synchrotron radiation. Annu Rev Mater Sci 22:121
11. Kak A, Slaney M (1988) Principles of Computerized Tomographic Imaging. IEEE Press, New York
12. Babout L, Maire E, Buffière JY, Fougères R (2001) Characterisation by X-ray computed tomography of decohesion, porosity growth and coalescence in model metal matrix composites. Acta Mater 49:2055
13. Borbély A, Csikor FF, Zabler S, Cloetens P, Biermann H (2004) Three-dimensional characterization of the microstructure of a metal-matrix composite by holotomography. Mater Sci Engng A 367:40
14. Kenesei P, Biermann H, Borbély A (2005) Structure–property relationship in particle reinforced metal-matrix composites based on holotomography. Scr Mater 53:787
15. Weck A, Wilkinson DS, Maire E, Toda H (2008) Visualization by x-ray tomography of void growth and coalescence leading to fracture in model materials. Acta Mater 56:2919
16. Toda H, Yamamoto S, Kobayashi M, Uesugi K, Zhang H (2008) Direct measurement procedure for three-dimensional local crack driving force using synchrotron X-ray microtomography. Acta Mater 56:6027
17. Williams JJ, Flom Z, Amell AA, Chawla N, Xiao X, De Carlo F (2010) Damage evolution in SiC particle reinforced Al alloy matrix composites by X-ray synchrotron tomography. Acta Mater 58:6194
18. Williams JJ, Yazzie KE, Phillips NC, Chawla N, Xiao X, De Carlo F, Iyyer N, Kittur M (2011) On the correlation between fatigue striation spacing and crack crowth rate: a three-dimensional (3-D) X-ray synchrotron tomography study. Metall Mater Trans 42:3845
19. Williams JJ, Yazzie KE, Phillips NC, Chawla N, Xiao X, De Carlo F Understanding fatigue crack growth in aluminum alloys by in situ x-ray synchrotron tomography. Int J Fatigue, in press
20. Groeber M, Ghosh S, Uchic MD, Dimiduk DM (2008) A framework for automated analysis and simulation of 3D polycrystalline microstructures. I: statistical characterization. Acta Mater 56:1257
21. Groeber M, Ghosh S, Uchic MD, Dimiduk D (2008) A framework for automated analysis and simulation of 3D polycrystalline microstructures. II: synthetic structure generation. Acta Mater 56:1274
22. Jiao Y, Stillinger FH, Torquato S (2007) Modeling heterogeneous materials via two-point correlation functions: basic principles. Phys Rev E 76:031110
23. Jiao Y, Stillinger FH, Torquato S (2008) Modeling heterogeneous materials via two-point correlation functions: II. Algorithmic details and applications. Phys Rev E 77:031135
24. Jiao Y, Stillinger FH, Torquato S (2009) A superior descriptor of random textures and its predictive capacity. Proc Natl Acad Sci 106:17634
25. Yeong CLY, Torquato S (1998) Reconstructing random media. Phys Rev E 57:495

26. Yeong CLY, Torquato S (1998) Reconstructing random media: II. Three-dimensional reconstruction from two-dimensional cuts. Phys Rev E 58:224
27. Liu Y, Greene MS, Chen W, Dikin DA, Liu WK (2013) Computational microstructure characterization and reconstruction for stochastic multiscale material design. Computer-Aided Design 45:65
28. Mikdam A, Belouettar R, Fiorelli D, Hu H, Makradi A (2013) A tool for design of heterogeneous materials with desired physical properties using statistical continuum theory mater. Sci Eng A 564:493
29. Jiao Y, Pallia E, Chawla N (2013) Modeling and predicting microstructure evolution in lead/tin alloy via correlation functions and stochastic material reconstruction. Acta Mater 61:3370
30. Roberts AP (1997) Statistical reconstruction of three-dimensional porous media from two- dimensional images Phys. Rev E 56:3203–12
31. Niezgoda SR, Kanjaria RK, Kalidindi SR (2013) Novel microstructure quantification framework for databasing, visualization, and analysis of microstructure data. Inter Mater Manu Innov 2:3
32. Niezgoda SR, Fullwood DT, Kalidindi SR (2008) Delineation of the space of 2-point correlations in a composite material system. Acta Mater 56:5285–92
33. Lu B, Torquato S (1992) Lineal path function for random heterogeneous materials. Phys Rev A 45:922
34. Lu B, Torquato S (1992) Lineal path function for random heterogeneous materials II. Effect of polydispersivity. Phys Rev A 45:7292
35. Torquato S, Beasley JD, Chiew YC (1988) Two-point cluster function for continuum percolation. J Chem Phys 88:6540
36. Cinlar E, Torquato S (1995) Exact determination of the two-point cluster function for one-dimensional continuum percolation. J Stat Phys 78:827
37. Torquato S (1986) Interfacial surface statistics arising in diffusion and flow problems in porous media. J Chem Phys 85:4622
38. Torquato S, Avellaneda M (1991) Diffusion and reaction in heterogeneous media: pore-size distribution, relaxation rimes, and mean survival time. J Chem Phys 95:6477
39. Prager S (1963) Interphase transfer in stationary two-phase media. Chem Eng Sci 18:228
40. Fullwood DT, Niezgoda SR, Kalidindi SR (2008) Microstructure reconstructions from 2-point statistics using phase-recovery algorithms. Acta Mater 56:942–48
41. Hajizadeh A, Safekordi A, Farhadpour FA (2011) A multiple-point statistics algorithm for 3D pore space reconstruction from 2D images. Advances in Water Resources 34:1256–1267
42. Tahmasebi P, Sahimi M (2013) Cross-correlation function for accurate reconstruction of heterogeneous media Phys. Rev Lett 110:078002
43. Sheehan N, Torquato S (2001) Generating microstructures with specified correlation functions. J Appl Phys 89:53
44. Rozman MG, Utz M (2002) Uniqueness of reconstruction of multiphase morphologies from two-point correlation functions. Phys Rev Lett 89:135501
45. Kirkpatrick S, Gelatt CD, Vecchi MP (1983) Optimization by simulated annealing. Science 220:671–80
46. Singh SS, Williams JJ, Jiao Y, Chawla N (2012) Modeling anisotropic multiphase heterogeneous materials via directional correlation functions: simulations and experimental verification metall. Mater Trans 4A:4470–4474
47. Debye P, Anderson HR, Brumberger H (1957) Scattering by an inhomogeneous solid. II. The correlation function and its applications. J Appl Phys 28:679–83
48. Manko HH (2001) Solders and Soldering: Materials, Design, Production, and Analysis for Reliable Bonding. McGraw-Hill, New York
49. Porter DA, Easterling KE (2004) Phase Transformations in Metals and Alloys. Taylor & Francis, London
50. Guo EY, Chawla N, Jing T, Torquato S, Jiao Y (2014) Accurate modeling and reconstruction of three-dimensional percolating filamentary microstructures from two-dimensional micrographs via dilation-erosion method. Mater Chara 89:33–42

doi:10.1186/2193-9772-3-3
Cite this article as: Jiao and Chawla: **Three dimensional modeling of complex heterogeneous materials via statistical microstructural descriptors.** *Integrating Materials and Manufacturing Innovation* 2014 **3**:3.